Effect of Tensor Force on the Halo Structure of ^{29}Ne and ^{31}Ne

2014 Commun. Theor. Phys. 61 101

(http://iopscience.iop.org/0253-6102/61/1/16)

Effect of Tensor Force on the Halo Structure of ^{29}Ne and ^{31}Ne*

QIU Chen (邱晨) and ZHOU Xian-Rong (周先荣)†

Department of Physics and Institute of Theoretical Physics and Astrophysics, Xiamen University, Xiamen 361005, China

(Received August 13, 2013; revised manuscript received September 4, 2013)

Abstract *The structure of Ne isotopes has been investigated by using deformed Skyrme–Hartree–Fock (SHF) method and BCS approximation. Especially the effect of tensor force on the halo structure of ^{29}Ne and ^{31}Ne is discussed. To this end, the tensor contributions are considered to the energy density function and the single particle potential in SHF theory. For comparison, four Skyrme interactions are used: SLy5 and SGII without tensor force, and SLy5+T and SGII+T with tensor force. The results indicate that the inclusion of tensor force shows a more pronounced halo structure for ^{31}Ne.*

PACS numbers: 21.10.Gv, 21.10.Dr, 21.10.Pc, 21.60.Jz
Key words: tensor force, halo structure, Skyrme–Hartree–Fock

1 Introduction

During last few decades, structures of exotic nuclei have been extensively studied theoretically and experimentally. Especially the studies on light exotic nuclei have revealed a lot of interesting phenomena, such as neutron halos and skins, prediction of proton halos, and cluster-like structure. The neutron halo is weakly bound exotic nuclear state where the valence neutrons are spatially decoupled from a tightly bound core and the wave function extends into the classically forbidden region. Interaction cross sections and reaction cross section can indicate the size of nuclei.[1−2] Based on this property, the neutron halo has been found in some neutron-rich nuclei. Experimentally, ^{11}Li is the first recognized neutron halo nucleus by Tanihanta *et al.*[1] Since then, a lot of neutron halo nuclei have been observed experimentally (see, for example, Refs. [3–5]). Theoretically, the neutron halo structure has been investigated by different models.[6−14]

Recently, the interaction cross sections for Ne isotopes from the stability line to the neutron drip line were measured[15] experimentally. The larger interaction cross sections for ^{29}Ne and ^{31}Ne were observed compared to their neighboring nuclei.[15−16] The analysis suggests an s dominant halo structure of ^{29}Ne and s- or p-orbit halo in ^{31}Ne.[15] Theoretically, the dependence of the reaction cross section on the ground state of the deformed halo nucleus ^{31}Ne was investigated by using the Glauber theory.[17]

The Ne isotopes around $N = 20$ also make up the so-called island of inversion.[18] In Ref. [18], the evidence for the presence of an anomaly in binding energies for the "island of inversion" centered at $Z = 11$, $N = 21$ is obtained by comparison of shell-model calculations to experiment. Recently, the deformation of Ne isotopes in the region of the island of inversion was determined by folding model description of the interaction cross sections measured for $^{28−32}$Ne isotopes.[19] The calculation indicates ^{31}Ne is a halo nucleus with large deformation around $\beta_2 = 0.4$.

Another topic about the neon isotopes is the shell structure in this region since they are across the sd neutron shell. Experimentally and theoretically, the appearance of new magic number $N = 14$ or $N = 16$ was widely studied (see Refs. [20–21] and references therein). In Ref. [22], the shell structure of neon isotopes was discussed by investigating the charge radii and a magic number is suggested in the middle of the sd shell.

On the other hand, one of the current topics is the role of the tensor interaction on the shell evolution of nuclei far from the stability. The experimental isospin dependence of the spin-orbit splittings in the $N = 82$ isotones and $Z = 50$ isotopes can not be described by the Skyrme–Hartree–Fock (SHF) calculations with standard Skyrme interactions, but is well reproduced by including the tensor interaction.[23] In Ref. [24], the effect of tensor interaction is studied on deformation and shell structure of various nuclei within the deformed SHF+BCS model. It is shown that $Z = 114$ and $N = 164$ shell gaps are more pronounced by the tensor correlations of SLy5+T interaction.

In Ref. [12], the deformation effect on the structure of $N = 7$ halo nuclei was discussed by using deformed SHF+BCS theory. In this paper, the shell structure of neon isotopes and the halo structure of ^{29}Ne and ^{31}Ne are investigated by using the same theory as in Ref. [12], but the tensor correlation is considered. Although there are some arguments[13−14,25−28] that in dealing with pairing correlation the BCS method is weaker in describing halo structure than the other approaches, the current studies

*Supported by National Natural Science Foundation of China under Grant Nos. 10975116 and 11275160
†E-mail: xrzhou@xmu.edu.cn

focus on the effect of tensor force on halo structure of ^{29}Ne and ^{31}Ne.

This paper is organized as follows. A brief introduction about SHF theory and tensor force is given in Sec. 2. We study the shell structure of Ne isotopes, the halo structure of ^{29}Ne and ^{31}Ne and the effect of tensor force in Sec. 3. A summary is given in Sec. 4.

2 Formalism

To minimize the total energy of nuclear system, we solve the Skyrme–Hartree–Fock (SHF) Schrodinger equation,[29]

$$\Big[-\vec{\bigtriangledown}\cdot\frac{h}{2m_q^\star(r)}\vec{\bigtriangledown}+U_q(\vec{r})+W_q(\vec{r})\cdot(-\mathrm{i})(\vec{\bigtriangledown}\times\sigma)\Big]\phi_i = e_i\phi_i\,, \tag{1}$$

taking into account the triplet-even and triplet-odd zero-range tensor interactions,

$$\begin{aligned} V_T = \frac{T}{2}\Big\{&\Big[(\boldsymbol{\sigma}_1\cdot\boldsymbol{k}')(\boldsymbol{\sigma}_2\cdot\boldsymbol{k}')-\frac{1}{3}\boldsymbol{k}'^2(\boldsymbol{\sigma}_1\cdot\boldsymbol{\sigma}_2)\Big]\\ &+\Big[(\boldsymbol{\sigma}_1\cdot\boldsymbol{k})(\boldsymbol{\sigma}_2\cdot\boldsymbol{k})-\frac{1}{3}(\boldsymbol{\sigma}_1\cdot\boldsymbol{\sigma}_2)\boldsymbol{k}^2\Big]\Big\}\delta(\boldsymbol{r}_1-\boldsymbol{r}_2)\\ &+U\Big\{(\boldsymbol{\sigma}_1\cdot\boldsymbol{k}')\delta(r_1-r_2)(\boldsymbol{\sigma}_2\cdot\boldsymbol{k})\\ &-\frac{1}{3}(\boldsymbol{\sigma}_1\cdot\boldsymbol{\sigma}_2)[\boldsymbol{k}'\cdot\delta(\boldsymbol{r}_1-\boldsymbol{r}_2)\boldsymbol{k}]\Big\}\,, \end{aligned} \tag{2}$$

where $\boldsymbol{k}$ and $\boldsymbol{k}'$ are the momentum operators acting on right and left hand side, respectively. The time-even and time-odd tensor coupling constants T and U are free parameters in the SHF model. For details, please refer to Ref. [24].

The vector part of the spin-orbit density in the SHF energy density is written as,

$$\triangle H=\frac{1}{2}\alpha(\vec{J}_n+\vec{J}_p)+\beta\vec{J}_n^2\vec{J}_p^2\,, \tag{3}$$

where

$$\alpha=\alpha_C+\alpha_T,\quad \beta=\beta_C+\beta_T\,, \tag{4}$$

including the contributions of central exchange and tensor term. α_C and β_C are written in terms of standard Skyrme parameters, while α_T and β_T are related to the tensor interactions (see Eq. (2)),

$$\begin{aligned} \alpha_C&=\frac{1}{8}(t_1-t_2)=\frac{1}{8}(t_1x_1+t_2x_2)\,,\\ \beta_C&=-\frac{1}{8}(t_1x_1+t_2x_2)\,,\\ \alpha_T&=\frac{5}{12}U,\quad \beta_T=\frac{5}{24}(T+U)\,. \end{aligned} \tag{5}$$

Beyond the mean field approximation, we consider the pairing interaction with BCS approximation. We take a density-dependent pairing interaction

$$V=V_0\Big(1-\frac{\rho(\vec{r_1}+\vec{r_2})/2}{\rho_0}\Big)^\lambda\cdot\delta(\vec{r_1}-\vec{r_2})\,, \tag{6}$$

where $\lambda=1$, and the reference density ρ_0 is taken as a standard value of 0.16 fm^{-3}.

3 Result and Discussion

We perform the deformed SHF+BCS calculations for Ne isotopes including the tensor contributions to the energy density function and also to the single particle potential. For odd-neutron nuclei, the blocking effect of odd neutron was taken into account. In order to study the effect of tensor force on the halo structure of ^{29}Ne and ^{31}Ne, we choose four different Skyrme interactions: SLy5 and SGII without tensor interaction, and SLy5+T,[23] SGII+T[30] with tensor interaction. In the calculation, the pairing strength is taken as $V_0=-410$ MeV$\cdot$fm^{-3} for neon isotopes as in Ref. [31].

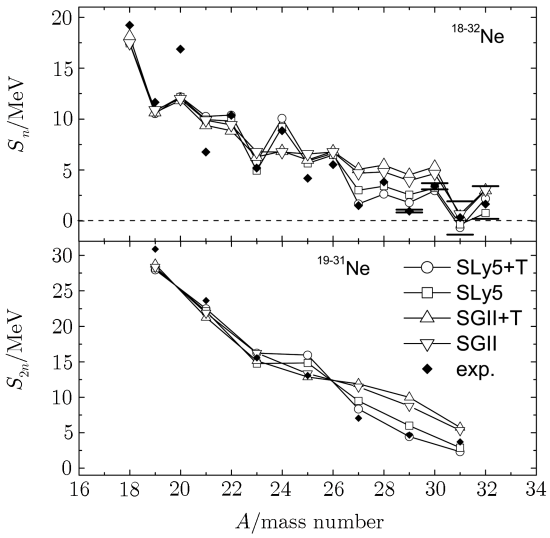

Fig. 1 Single and double neutron separation energies for Ne isotopes as a function of neutron number. The top and bottom panel show single and double neutron separation energies, respectively. The Experimental data are indicated by filled diamonds. The results for the SLy5, SLy5+T, SGII, and SGII+T are indicated by open square, open circles, open down triangle, and open upper triangle, respectively.

Figure 1 shows the calculated single neutron separation energies S_n (top panel) and double neutron separation energies S_{2n} (bottom panel) for Ne isotopes, with comparison to the experimental data. The neon isotopes span the whole sd shell across the magic number $N=8$ and $N=20$. Currently, the new magic numbers such as $N=14$ or $N=16$ are widely discussed in the literatures both from experimental and theoretical side (see Refs. [20–21] and references therein). From Fig. 1, we see that for all four Skyrme interactions, there is a big gap of S_n at the $N=8$ magic number. In the middle of sd shell, there are several gaps such as $N=12$, $N=14$, and $N=16$, which agree with the investigation of the charge radii of neon isotopes in Ref. [22]. Compared to the results of SLy5 interaction the calculation with SLy5+T interaction gives a clear $N=16$ gap, and the amplitude is comparable to the gap at $N=20$. Both the calculation with SGII and

SGII+T interaction can not give an $N = 14$ or $N = 16$ gap, but an $N = 12$ gap instead.

The calculated single particle separation energies and experimental data for ^{29}Ne and ^{31}Ne are listed in Table 1. In the case of ^{29}Ne, compared to the experiment, the results with SLy5 or SLy5+T are better than those of SGII or SGII+T interaction, while for ^{31}Ne, due to the large error bar from experiment, all the calculations agree well with the experimental data. However, in the case of SLy5 or SLy5+T interaction, the ^{31}Ne is a neutron emission nucleus.

Table 1 The calculated one-neutron separation energy and experimental data for ^{29}Ne and ^{31}Ne in the unit of MeV. The experimental data are from Ref. [33].

	SGII	SGII+T	SLy5	SLy5+T	Exp
^{29}Ne	3.594	4.525	2.562	1.802	0.95 ± 0.15
^{31}Ne	0.659	0.418	−0.335	−0.668	0.29 ± 1.6

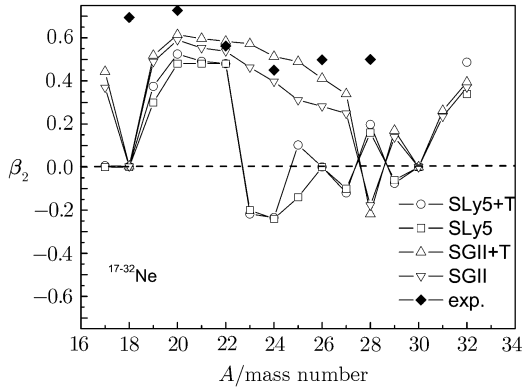

Fig. 2 The calculated β_2 deformation parameters versus mass number from the quadrupole moments obtained from SHF calculations. The Experimental data are reprsented by filled diamonds. The results for the SLy5, SLy5+T, SGII, and SGII+T are given by open square, open circles, open down triangle, and open upper triangle, respectively.

To investigate the shape evolution of neon isotopes, in Fig. 2 the calculated quadrupole deformation β_2 values are plotted as a function of mass number for SLy5, SLy5+T, SGII, and SGII+T interaction, respectively. For comparison, the experimental data are also given. All the calculations give a spherical shape at $A = 30$ due to the $N = 20$ closed shell. Experimentally, there is a deformation minimum at $A = 24$ in the middle of the sd shell corresponding to the closure of $d_{5/2}$ subshell.[32] The SLy5 and SLy5+T calculations give a β_2 minimum at $A = 26$ corresponding to the gap of S_n (see Fig. 1), indicating the $N = 16$ subshell. Compared with the experimental data, the results with SGII or SGII+T interaction agree better with the experiment than those of SLy5 and SLy5+T. We also notice that the tensor force in SGII interaction makes a big changes of β_2 for the nuclei $21 \leq A \leq 27$, while the shapes of SLy5 and SLy5+T calculation are nearly the same except at $A = 25$ due to shape coexistence in ^{25}Ne.

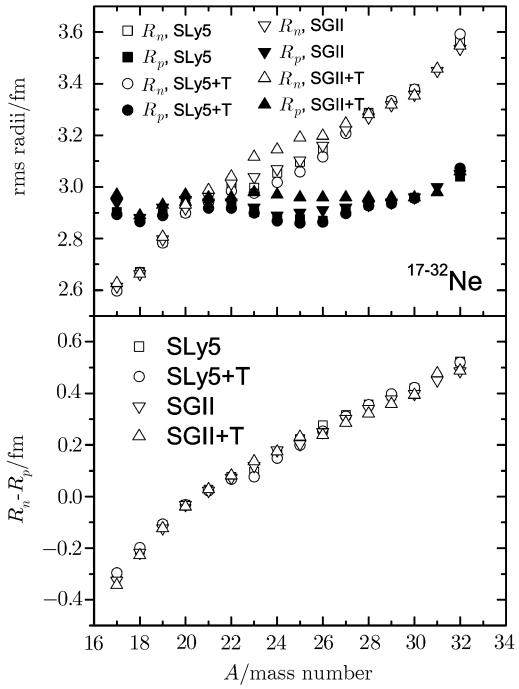

Fig. 3 (a) Rms neutron and proton radii (b) difference between rms neutron and proton radii of Ne isotopes as a function of atomic number. The solid signs represent proton radii. The open signs are the neutron radii.

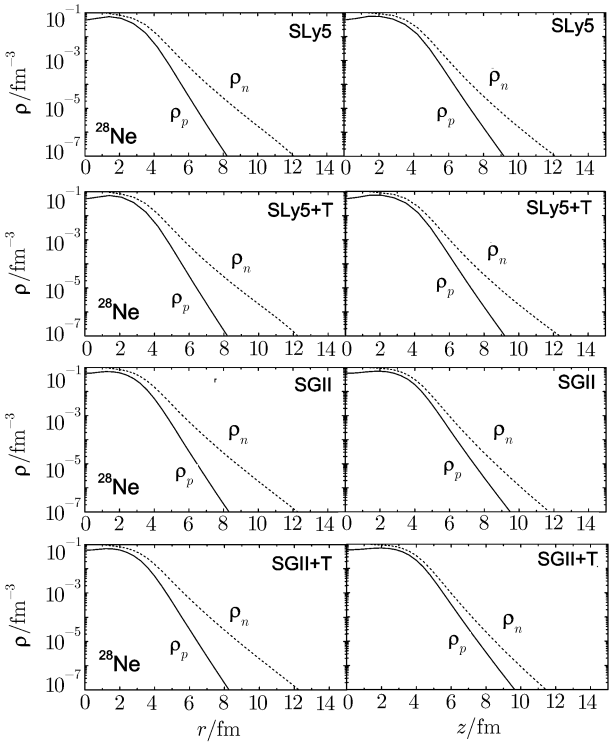

Fig. 4 Neutron and proton density distribution of ^{28}Ne as a function of r (left panel) and z (right panel) direction with (a) SLy5 at $\beta_2 = 0.16$ (b) SLy5+T at $\beta_2 = 0.20$ (c) SGII at $\beta_2 = 0.23$ and (d) SGII+T at $\beta_2 = -0.22$, respectively. The solid line and dashed line indicate the proton and neutron density, respectively.

To study the halo structure of neon isotopes, in Fig. 3, we plot the neutron and proton root-mean-square (rms) radii (upper panel) and the difference between the neutron and proton radii (lower panel) of Ne isotopes as a function of mass number. In upper panel, both the neutron and proton rms radii increase with A. The tensor force in SGII+T interaction makes a big change of radii in the nuclei $21 \leq A \leq 27$ corresponding to the changes of shapes. For SGII and SGII+T interaction, we see a jump for the $A = 31$ neutron radius and a corresponding jump in the difference of neutron and proton radii, which indicates the neutron halo structure in ^{31}Ne. It agrees with the experimental halo structure.[15] While for ^{29}Ne, the jump of neutron is not obvious for all four interactions.

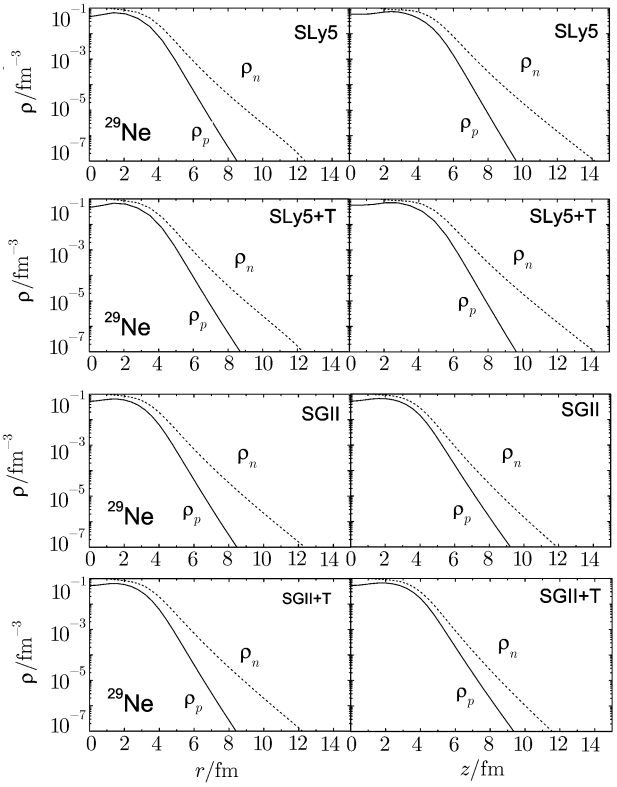

Fig. 5 The same as Fig. 4, but for ^{29}Ne with (a) SLy5 at $\beta_2 = -0.07$ (b) SLy5+T at $\beta_2 = -0.07$ (c) SGII at $\beta_2 = 0.14$ and (d) SGII+T at $\beta_2 = 0.17$, respectively.

In order to describe the density distribution of halo nuclei, it is suggested that the relativistic Hartree theory should be solved in coordinate space[34] or in the basis equivalent to coordinate space.[35] In current calculation, the axial symmetry is assumed and the SHF Eq. (1) is solved in cylinder coordinate space. In Figs. 4 and 5, the neutron and proton densities of ground states are given as a function of r and z direction for SLy5 ($\beta_2 = -0.07$), SLy5+T ($\beta_2 = -0.07$), SGII ($\beta_2 = 0.14$), and SGII+T ($\beta_2 = 0.14$), respectively. Compared to the density distribution of ^{28}Ne (Fig. 4), the ^{29}Ne density distributions of the calculations with SLy5 and SLy5+T Skyrme force show an exponentially extended tail, indicating the halo structure of this nucleus. The difference between the density distributions of ^{29}Ne in r and z direction indicates the deformed halo structure in this nucleus for SLy5 and SLy5+T interaction.

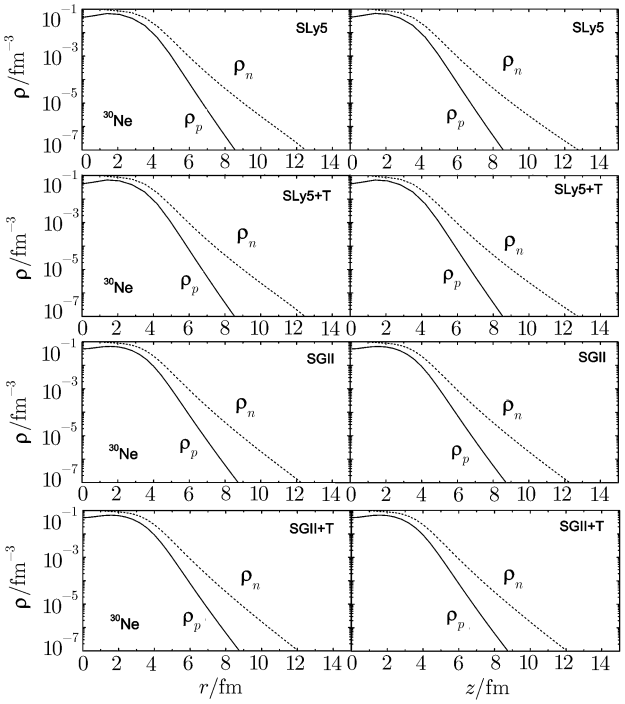

Fig. 6 The same as Fig. 4, but for ^{30}Ne with $\beta_2 = 0.0$.

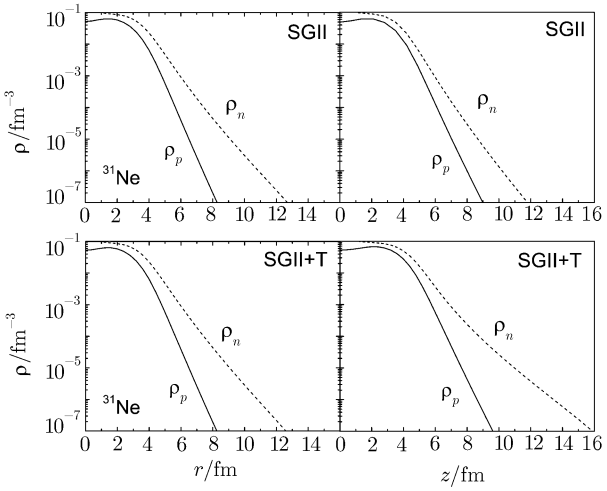

Fig. 7 The same as Fig. 4, but for ^{31}Ne with (a) SGII at $\beta_2 = 0.23$ (b) SGII+T at $\beta_2 = 0.20$.

Similarly, we plot in Fig. 6 the neutron and proton densities of ground states as a function of r and z direction for SLy5, SLy5+T, SGII, and SGII+T, respectively. Since for the above four Skyrme forces, only the SGII and SGII+T can produce a bound nuclear system. In Fig. 7, we only plot the neutron and proton densities as a function of r and z direction for SGII ($\beta_2 = 0.23$), and SGII+T

($\beta_2 = 0.20$), respectively. Only the density distribution of ^{31}Ne with SGII+T force shows an exponentially extended tail in comparison with to the density distribution of ^{30}Ne (Fig. 6), which indicates a halo structure for this nucleus. In this sense, the inclusion of tensor force can better reproduce the deformed halo structure of ^{31}Ne with $\beta_2 = 0.20$.

4 Summary

In summary, the deformed SHF+BCS method has been applied to study the structure of neon isotopes. The tensor contributions to the energy density function and the single particle potential are taken into account. The effect of tensor force on the halo structure of ^{29}Ne and ^{31}Ne is discussed. In the calculation, we choose four different Skyrme interactions: SLy5 and SGII without tensor interaction, and SLy5+T, SGII+T with tensor correlation. For ^{29}Ne, all the calculations can produce a bound system. Either the SGII or SGII+T can not produce a halo structure, while the calculation with SLy5 and SLy5+T interaction shows a very extended spatial density distribution indicating a halo structure in ^{29}Ne. In the case of ^{31}Ne, only SGII and SGII+T interaction can give a bound nuclear system. Compared to the results of SGII, the neutron density distribution with SGII+T interaction shows an exponentially extended tail at $\beta_2 = 0.20$, indicating a deformed halo structure. In other words, the deformed SHF + BCS calculation indicates that the inclusion of tensor force shows a more pronounced halo structure for ^{31}Ne.

References

[1] I. Tanihata, H. Hamagaki, O. Hashimoto, Y. Shida, and N. Yoshikawa, Phys. Rev. Lett. **55** (1985) 2676.

[2] A. Ozawa, *et al.*, Nucl. Phys. A **691** (2001) 599.

[3] T. Aumann, A. Navin, D.P. Balamuth, *et al.*, Phys. Rev. Lett. **84** (2000) 35.

[4] Y.L. Ye, D.Y. Pang, G.L. Zhang, *et al.*, J. Phys. G **31** (2005) S1647.

[5] P. Mueller, I.A. Sulai, A.C.C. Villari, *et al.*, Phys. Rev. Lett. **99** (2007) 252501.

[6] Z.Z. Ren, M. Mittig, B.Q. Chen, *et al.*, Phys. Rev. C **52** (1995) R1764.

[7] H. Sagawa, Phys. Lett. B **286** (1992) 7.

[8] J. Meng, Nucl. Phys. A **635** (1998) 31.

[9] J. Meng and P. Ring, Phys. Rev. Lett. **80** (1998) 460.

[10] Z.H. Liu, C.J. Lin, H.Q. Zhang, *et al.*, Phys. Rev. C **64** (2001) 034312.

[11] J. Meng, H. Toki, J.Y. Zeng, S.Q. Zhang, and S.G. Zhou, Phys. Rev. C **65** (2002) 041302(R).

[12] J.C. Pei, F.R. Xu, and P.D. Stevenson, Nucl. Phys. A **765** (2006) 29.

[13] S.G. Zhou, J. Meng, P. Ring, and E.G. Zhao, Phys. Rev. C **82** (2010) 011301(R).

[14] Lu-Lu Li, Jie Meng, P. Ring, En-Guang Zhao, and Shan-Gui Zhou, Phys. Rev. C **85** (2012) 024312.

[15] M. Takechi, M. Ohtdubo, M. Fukuda, *et al.*, Phys. Lett. B **707** (2012) 357.

[16] T. Nakamura, *et al.*, Phys. Rev. Lett. **103** (2009) 262501.

[17] Y. Urata, K. Hagino, and H. Sagawa, Phys. Rev. C **86** (2012) 044613.

[18] E.K. Warburton, J.A. Becker, and B.A. Brown, Phys. Rev. C **41** (1990) 1147.

[19] T. Sumi, K. Minomo, S. Tagami, *et al.*, Phys. Lett. B **707** (2012) 357.

[20] H. Grawe, in the *The Euroschool Lectures on Physics with Exotic Beams*, Vol. I, ed. by J. A1-Khalili and E. Roeckl, *Lect Notes. Phys.* **651** Springer, Berlin Heidelberg (2004) p. 33.

[21] O. Sorlin and M.G. Porquet, Prog. Part. Nucl. Phys. **61** (2008) 602.

[22] K. Marinova, W. Geither, M. Kowalska, *et al.*, Phys. Rev. C **84** (2011) 034313.

[23] G. Coló, H. Sagawa, S. Fracasso, and P.F. Bortignon, Phys. Lett. B **646** (2007) 227.

[24] Xian-Rong Zhou and H. Sagawa, J. Phys. G: Nucl. Part. Phys. **39** (2012) 085104.

[25] M.M. Sharma, G.A. Lalazissis, W. Hillebrandt, and P. Ring, Phys. Rev. Lett. **72** (1994) 1431.

[26] J. Meng and P. Ring, Phys. Rev. Lett. **77** (1996) 3963.

[27] J.C. Pei, Y.N. Zhang, and F.R. Xu, Phys. Rev. C **85** (2013) 024312.

[28] Shi-Sheng Zhang, En-Guang Zhao, and Shan-Gui Zhou, Eur. Phys. J. A **49** (2013) 77.

[29] D. Vautherin and D.M. Brink, Phys. Rev. C **5** (1972) 626.

[30] C.L. Bai, H.Q. Zhang, H. Sagawa, X.Z. Zhang, G. Colo, and F.R. Xu, Phys. Rev. C **83** (2011) 054316.

[31] H. Sagawa, Xian-Rong Zhou, Toshio Suzuki, and N. Yoshida, Phys. Rev. C **78** (2008) 041304(R).

[32] S. Raman, C.W. Nestor Jr., and P. Tikkanen, At. Data Nucl. Data Tables **78** (2001) 1.

[33] B. Jurado, H. Savajols, W. Mittig, *et al.*, Phys. Lett. B **649** (2007) 43.

[34] Shan-Gui Zhou, Jie Meng, Shuhei Yamaji, and Si-Chun Yang, Chin. Phys. Lett. **17** (2000) 717.

[35] Shan-Gui Zhou, Jie Meng, and P. Ring, Phys. Rev. C **68** (2003) 034323.